

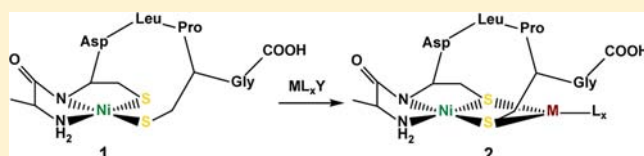
# Construction of Heterometallic Clusters in a Small Peptide Scaffold as [NiFe]-Hydrogenase Models: Development of a Synthetic Methodology

Arnab Dutta,<sup>†,‡</sup> G. Alexander Hamilton,<sup>†</sup> Hilairy Ellen Hartnett,<sup>†,§</sup> and Anne Katherine Jones<sup>\*,†,‡</sup>

<sup>†</sup>Department of Chemistry and Biochemistry, <sup>‡</sup>Center for Bio-Inspired Solar Fuel Production, and <sup>§</sup>School of Earth and Space Exploration, Arizona State University; Tempe, Arizona 85287, United States

## Supporting Information

**ABSTRACT:** [NiFe]-hydrogenases are enzymes that catalyze the reversible interconversion of protons and hydrogen at a heterobimetallic site containing Ni and Fe. This organometallic site has served as an inspiration for the synthesis of a number of biomimetic complexes, but, unfortunately, most close structural mimics have shown little to no reactivity with either of the substrates for hydrogenases. This suggests that interactions between the metallo-active site and the protein scaffold are crucial in tuning reactivity. As a first step toward development of peptide-based models, in this paper we demonstrate a synthetic strategy for construction of peptide coordinated, cysteinyl thiolate bridged Ni-M complexes in which M is a hetero-organometallic fragment. We utilize the seven amino acid peptide ACDLPCG as a scaffold for construction of these peptide-coordinated metalcenters. This peptide binds Ni in an N<sub>2</sub>S<sub>2</sub> environment consisting of the amino terminus, an amide nitrogen, and the two cysteinyl thiolates. We show that these thiolates serve as reactive sites for formation of heterometallic complexes in which they serve as bridging ligands. The method is general, and a number of heterometallic fragments including Ru( $\eta^6$ -arene)<sup>2+</sup>, M(CO)<sub>4</sub>(piperidine) for M = Mo and W, and Fe<sub>2</sub>(CO)<sub>6</sub> were successfully incorporated, and the resulting metallopeptides characterized via a range of spectroscopic techniques. This methodology serves as the first step to construction of hydrogenase peptidomimetics that incorporate defined outer coordination sphere interactions intended to tune reactivity.



## INTRODUCTION

Hydrogenases, the metalloenzymes responsible for the biological interconversion of hydrogen and protons, have received widespread attention for their potential uses in technological applications.<sup>1</sup> As shown in Figure 1, [NiFe]-hydrogenases feature a biologically unusual organometallic active site in which a tetrathiolate coordinated Ni shares two bridging cysteine thiolates (represented as SR) with an Fe(CO)(CN)<sub>2</sub> moiety.<sup>2,3</sup> This motif has inspired the synthesis of a rich variety of thiolate bridged Ni-M compounds that serve, to varying degrees, as

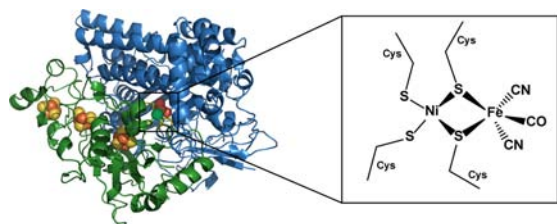


**Figure 1.** Overall ribbon structure of the [NiFe]-hydrogenase from *Desulfovibrio gigas* (PDB ID: 1FRV). The [NiFe] active site containing large subunit is shown in blue and the [FeS]-containing small subunit in green. Prosthetic groups are shown in ball and stick representation. The chemical structure of the active site is expanded in the black box. The figure was prepared using PyMOL software [The PyMOL Molecular Graphics System, Version 0.99rc6, Schrödinger, LLC].

structural or functional models of the enzyme active site.<sup>4,5</sup> The typical synthetic route to such compounds combines a Ni<sup>II</sup>(SR)<sub>2</sub> precursor with a heterofragment with labile ligands that can be exchanged for the thiolates. The identity of the second fragment can be quite diverse, encompassing mono- as well as bi- nuclear metalcenters and a wide range of ligand sets.<sup>6–11</sup>

Despite the intense interest in hydrogenases, many open questions remain regarding their mechanisms, and evidence is mounting that the protein matrix may play crucial roles in tuning the reactivity of the inorganic active site.<sup>12–14</sup> Artificial metalloproteins are proving to be a powerful tool for understanding metal-containing active sites at a molecular level and exploring the roles played by the protein matrix in modulating the physical properties of a metalcenter.<sup>15–24</sup> Although protein design has made the introduction of a single metal ion or preformed cofactors such as hemes or [FeS] clusters into an artificial scaffold more accessible, means for introducing multiple distinct metals and/or organometallic complexes are in their infancy.<sup>25–28</sup> Inspired by the A-cluster of acetylcoenzyme A synthase-carbon monoxide dehydrogenases, Holm and co-workers reported the first attempts to create peptide-coordinated, bridged assemblies in which two metalcenters, a mononuclear nickel center and a [4Fe4S] cluster

Received: December 13, 2011

Published: August 27, 2012



were connected by a covalent bridge, a cysteine ligand.<sup>25</sup> Similarly, Green and co-workers reported utilization of the resin bound peptide CGC as an  $N_2S_2$  coordinating ligand for nickel and its derivatization with  $W(CO)_5$  and  $Rh(CO)_2^+$  to produce heterobimetallic complexes.<sup>29</sup> However, this tripeptide provides little opportunity to tailor interactions with the metal center. To develop peptide models for [FeFe]-hydrogenases, methods have been developed to introduce  $[(\mu-SRS)[Fe(CO)_3]_2]$  derivatives into peptides using both natural cysteine and an artificial dithiol modification<sup>30–33</sup> but, to date, peptide-based models of [NiFe]-hydrogenases are scarce. Jain and co-workers have constructed mononuclear  $[Ni(P^{Ph}_2N^R)_2]^{2+}$  complexes in which R is a mono or dipeptide, but their synthetic strategy necessarily imposes 4-fold symmetry on the peptide components and prevents direct modification of the metal first coordination sphere.<sup>34</sup>

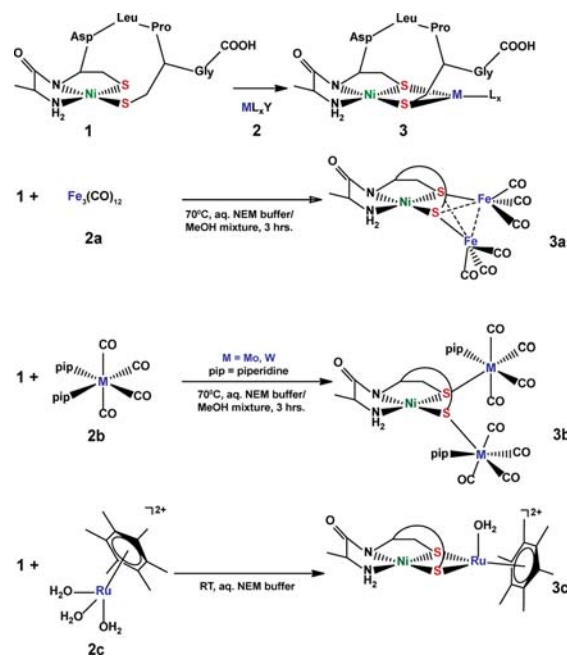
In this paper, we report the use of a small peptide as a scaffold for construction of heterometallic clusters. The enzyme nickel superoxide dismutase (NiSOD) binds a mononuclear Ni(II) in a square-planar  $N_2S_2$  first coordination sphere consisting of two cysteinyl thiolates, the amino terminus of the protein, and an amide nitrogen derived from the protein backbone. Oxidation of the Ni center to Ni(III) induces binding of the N-terminal histidine and a change to a square-based pyramidal geometry.<sup>35–37</sup> Interestingly, most of the interactions critical for binding Ni to this protein are provided by the first seven amino acids in the sequence: HCDLPCG. In fact, Neupane and co-workers demonstrated that this heptapeptide alone is sufficient to coordinate Ni, and the resulting complex maintained superoxide dismutase activity. Furthermore, replacement of the axial histidine ligand by alanine did not prevent formation of the Ni complex although the loss of the fifth ligand destabilized the Ni(III) state.<sup>38</sup> Here, we report the utilization of Ni-coordinated ACDLPCG, the alanine variant of the Ni-binding hook that we will refer to as NiSODA, as a fragment for construction of [NiFe]-hydrogenase models. As shown in Scheme 1, the cysteinyl thiolates of this metalloprotein can exchange labile ligands on heterometallic complexes. Synthesis and characterization of a range of model complexes for [NiFe]-hydrogenases of different metal composition, nuclearity, and terminal ligand set will be presented, demonstrating the generality of this methodology for production of peptide-based heterobimetallic complexes.

## EXPERIMENTAL SECTION

**General Procedures.** All inorganic syntheses were performed on a double-manifold Schlenk vacuum line under a nitrogen atmosphere. Unless otherwise specified, all chemicals and solvents were obtained from Sigma-Aldrich and were of the highest grade available. Aqueous solutions were prepared using purified water (resistivity 18.2 M $\Omega$ ·cm).

**Physical Measurements.** MALDI-MS (matrix-assisted laser desorption/ionization-mass spectrometry) characterization of peptides was performed on a Voyager DE STR in the Proteomics and Protein Chemistry Laboratory at Arizona State University using  $\alpha$ -Cyano-4-hydroxycinnamic acid in acetonitrile/water (50:50 by volume) as the matrix. ESI-MS (electrospray ionization-mass spectrometry) was performed using a Thermo Quantum Discovery Max triple-quadrupole mass spectrometer in the Environmental Biogeochemistry Laboratory at Arizona State University. Measurements were conducted in positive (+) and negative (–) ionization modes using a methanol/water (50:50 by volume) mobile phase at a flow rate of 10  $\mu$ L min<sup>–1</sup> and the following ionization conditions: spray voltage, 4000 (+, –); capillary temperature, 270 °C; sheath gas pressures, 25 (+) and 15 (–); auxiliary gas pressure, 2 (+, –). Isotope pattern calculator v4.0 (developed by Junhua Yan) was used to simulate the molecular mass

**Scheme 1.** General Synthetic Strategy for the Synthesis of Heterometallic Ni-M (M = Ru, Fe<sub>2</sub>, W, and Mo) Complexes in SODA<sup>a</sup>



<sup>a</sup> $L_x$  generally represents  $\pi$ -accepting ligands, and Y represents readily exchangeable ligands. The specific reactions demonstrated in this paper are shown here.

spectral data. NMR spectra were recorded at 400 MHz (<sup>1</sup>H) using Varian Liquid-State NMR instruments in CDCl<sub>3</sub> solutions (99.8%, Cambridge Isotopes Laboratories Inc.) containing 0.1% TMS (tetramethylsilane) or in D<sub>2</sub>O (99.9%, Cambridge Isotopes Laboratories Inc.) unless otherwise noted. UV–vis measurements were performed using a Hewlett-Packard 8453 spectrophotometer using quartz cuvettes with a 1 cm path length. FTIR (Fourier transformed infrared) spectra were recorded on a Thermo Nicolet Avatar-360 spectrometer either as KBr pellets or as a dry film on a CaF<sub>2</sub> window. Each spectrum is an average of 250 scans (for KBr pellets) or 264 scans (for dry film samples) at 1 cm<sup>–1</sup> resolution. Circular dichroism (CD) spectroscopy was performed on a Jasco 710 or J-815 spectropolarimeter using a rectangular quartz cell with a path length of 0.1 cm. Metal concentrations were determined using inductively coupled plasma mass spectrometry (ICP-MS) on a Thermo Finnigan X-Series quadrupole ICP-MS in CCT mode (for Fe) and normal mode (for Ni, Mo, Ru, and W), using 7% H<sub>2</sub> in He as the collision cell gas. Indium, bismuth, and germanium were used as internal standards. Iron was measured at masses 54, 56, and 57 and Ni at masses 58 and 60, molybdenum at 95 and 97, ruthenium at 101 and 102, and tungsten at 182 and 184. Samples were digested in concentrated nitric acid in Teflon beakers. After digestion, samples were dried and dissolved in 0.32 M HNO<sub>3</sub> for measurements. XPS data were acquired using a VG 220i-XL system. The X-ray source uses a monochromated Al K $\alpha$  line at 1486.6 eV. The base pressure of the system is 7  $\times$  10<sup>–10</sup> mbar, and spectra were acquired at approximately 1  $\times$  10<sup>–9</sup> mbar. Powder samples were pressed into indium (In) foil for transfer into the system. X-ray photoelectron spectroscopy (XPS) spectra were calibrated to the C1s peak position (at 285.0 eV for CH<sub>3</sub>) and analyzed using CasaXPS software (version 2.3.15, Casa Software Ltd.).

**Peptide Synthesis and Purification.** The seven amino acid peptide referred to as SODA (ACDLPCG) was synthesized on a Protein Technologies PS3 automated peptide synthesizer using the standard Fmoc/tBu (Fmoc, 9-fluorenylmethoxycarbonyl) protection strategy and HBTU (o-benzotriazole-*N,N,N',N'*-tetramethyluronium hexafluorophosphate) as coupling agent on Fmoc-glycine resin at 0.4 mmol scale. Fmoc protected amino acids, Fmoc-Glycine resin,

and HBTU were obtained from Protein Technologies (Tucson, AZ, U.S.A.). The peptide was simultaneously deprotected and cleaved from the resin using a mixture of 94% TFA (trifluoroacetic acid), 2.5% water, 2.5% EDT (ethanedithiol), and 1% TIPS (triisopropylsilane) for 2 h. Following concentration, the crude peptide was precipitated by adding cold ( $-20\text{ }^{\circ}\text{C}$ ) diethyl ether. The crude peptide was purified by reverse-phase HPLC on a Waters 600E system with a photodiode array detector on either a  $3 \times 250\text{ mm}$  ODS-A,  $300\text{ \AA}$  C-18 column from YMC Inc. for analytical scale or a PrepLC 25 mm module C-18 column from Waters for semipreparative scale. Aqueous acetonitrile gradients containing 0.1% TFA (v/v) were used as the mobile phase. Sample purity was confirmed by analytical HPLC and molecular weight determined by MALDI-MS. Since the peptide does not contain a convenient chromophore, peptide concentrations were quantified using the Ellman procedure that measures thiol content.<sup>39</sup>

**Metallopeptide Complexes Synthesis.** *NiSODA*. NiSODA was synthesized in 50 mM *N*-ethylmorpholine (NEM) buffer (pH 7.5) from  $\text{NiCl}_2$  (anhydrous) as described in reference 33. The concentration of NiSODA was determined spectroscopically using  $\epsilon_{459} = 427\text{ M}^{-1}\text{ cm}^{-1}$  and purity confirmed via analytical HPLC (Supporting Information, Figure S1).

*NiSODA-Fe<sub>2</sub>(CO)<sub>6</sub>*. Ten milligrams of  $\text{Fe}_3(\text{CO})_{12}$  in 3 mL of MeOH was added to 2.5 mL of 1.2 mM solution of NiSODA in 50 mM NEM buffer, pH 7.5, and stirred at room temperature for 15 min. The mixture was subsequently heated to  $70\text{ }^{\circ}\text{C}$  for 2.5 h. The solution turned reddish brown. After cooling, the solution was centrifuged and filtered through  $0.8/0.2\text{ }\mu\text{m}$  Acrodisc syringe filter (Pall corporation) to remove the green precipitate. The solution was evaporated under reduced pressure to remove the methanol. The remaining aqueous solution was purified by analytical HPLC (0–100% acetonitrile gradient in water). The purified NiSODA- $\text{Fe}_2(\text{CO})_6$  sample was lyophilized and then rehydrated to the desired concentration before spectroscopic characterization. As a control experiment, an analogous reaction between SODA and  $\text{Fe}_3(\text{CO})_{12}$  was also performed. After reaction, the SODA- $\text{Fe}_2(\text{CO})_6$  complex was isolated by filtering unreacted  $\text{Fe}_3(\text{CO})_{12}$  and removing the methanol under reduced pressure.

*NiSODA-[Mo(CO)<sub>4</sub>(piperidine)]<sub>2</sub> and NiSODA-[W(CO)<sub>4</sub>(piperidine)]<sub>2</sub>*. NiSODA- $[\text{M}(\text{CO})_4(\text{piperidine})]_2$  (M = Mo, W) complexes were prepared via two different methods. First, one equivalent (2.5 mg) of  $\text{W}(\text{CO})_4(\text{piperidine})_2$  was dissolved in 50 mL of methanol. This anaerobic solution was then added slowly to a 2 mL solution of 2.68 mM NiSODA in 50 mM NEM buffer (pH 7.5) at room temperature. The mixture was then refluxed ( $65\text{ }^{\circ}\text{C}$ ) for 2 h. After cooling, the methanol was removed under reduced pressure, and the remaining aqueous solution was lyophilized to obtain a solid powder. Unreacted  $\text{W}(\text{CO})_4(\text{piperidine})_2$  was removed by dissolving the mixture in water and filtering out the insoluble  $\text{W}(\text{CO})_4(\text{piperidine})_2$ . The water-soluble part was then purified via HPLC. NiSODA- $[\text{Mo}(\text{CO})_4(\text{piperidine})]_2$  was also synthesized using an analogous procedure. In the second method, a concentrated sample of  $\text{M}(\text{CO})_4(\text{piperidine})_2$  was prepared in *N,N'*-dimethylformamide (DMF). Then one equivalent of NiSODA in aqueous NEM buffer (pH 7.5) was added to the solution at room temperature. After addition, the v/v ratio of aqueous solution to DMF was 20:1. The mixture was heated at  $65\text{ }^{\circ}\text{C}$  for 2 h, and the rest of the experiment was performed as for the first method. Both methods gave comparable results.

*[NiSODA-Ru( $\eta^6$ -p-cymene)(H<sub>2</sub>O)<sub>3</sub>](NO<sub>3</sub>)<sub>2</sub> and [NiSODA-Ru( $\eta^6$ -C<sub>6</sub>Me<sub>6</sub>)(H<sub>2</sub>O)<sub>3</sub>](NO<sub>3</sub>)<sub>2</sub>*.  $\text{Ru}(\eta^6\text{-p-cymene})(\text{H}_2\text{O})_3(\text{NO}_3)_2$  was prepared as described in reference 35. Similarly,  $[\text{Ru}(\eta^6\text{-C}_6\text{Me}_6)(\text{H}_2\text{O})_3](\text{NO}_3)_2$  was prepared as described in reference 36. A 1 mL aqueous solution of 3.3 mM  $\text{Ru}(\eta^6\text{-arene})(\text{H}_2\text{O})_3^{2+}$  (arene = C<sub>6</sub>Me<sub>6</sub> or *p*-cymene) was added to 3 mL of 1.1 mM NiSODA in 50 mM NEM, pH 7.5 buffer and stirred at room temperature for 4 h. Purification of the complexes was achieved using reversed phase HPLC on the analytical scale. Aqueous acetonitrile gradients (0–100%, without TFA) were used as the mobile phase. The acetonitrile concentration was increased at a rate of  $1\text{ min}^{-1}$  and the flow rate was  $0.5\text{ mL min}^{-1}$ . Purified  $[\text{NiSODA-Ru}(\eta^6\text{-C}_6\text{Me}_6)(\text{H}_2\text{O})_3](\text{NO}_3)_2$  eluted from the column at

27.0 min. See also Supporting Information, Figure S13 for chromatograms.

## RESULTS AND DISCUSSION

The general strategy developed in this work for the synthesis of peptide coordinated heterometallic (Ni-M) complexes is summarized in Scheme 1. First, Ni was incorporated into purified SODA in 50 mM NEM buffer at pH 7.5 as described by Neupane and co-workers.<sup>38</sup> Metal incorporation was confirmed by UV-vis spectroscopy [ $\epsilon_{459\text{ nm}}(\text{NiSODA}) = 427\text{ M}^{-1}\text{ cm}^{-1}$ ] (Figure 2) and MALDI mass spectrometry

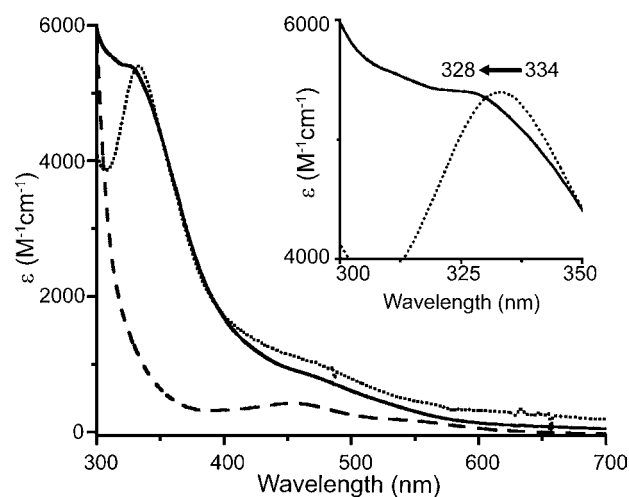


**Figure 2.** UV-vis spectra from NiSODA (dashed line), SODA- $\text{Fe}_2(\text{CO})_6$  (dotted line), and NiSODA- $\text{Fe}_2(\text{CO})_6$  (solid line). Spectra were recorded in 50 mM aqueous NEM buffer (pH 7.5). In the inset, the MLCT band region is magnified to show the difference between SODA- $\text{Fe}_2(\text{CO})_6$  (dotted line) and NiSODA- $\text{Fe}_2(\text{CO})_6$  (solid line).

(Supporting Information, Figure S2). NiSODA was then used as a metalloligand for exchange reactions with iron, tungsten, molybdenum, and ruthenium complexes with labile ligands. When considering this general synthetic strategy, two properties of NiSODA are important to note. First, NiSODA is only sparingly soluble in organic solvents. Second, Ni is coordinated to SODA only at circumneutral pH (6–8). If the pH is too high, insoluble nickel(II) hydroxide forms, and, if the solution is too acidic, the cysteinyl ligands are not deprotonated. Thus, one of the unique challenges of preparing organometallic peptide complexes of this type is identifying appropriate solvents for both components of the reaction.

**NiFe Complexes.** Metal carbonyls have been used to great effect in models of hydrogenases with the advantage that FTIR spectroscopy can be employed to probe the resulting complexes. Schröder and co-workers described the synthesis and reactivity of a trimetallic  $[\text{Ni}(\mu\text{-SR})_2\text{Fe}_2(\text{CO})_6]$  cluster by reaction of a nickel tetrathiolate complex with  $\text{Fe}_3(\text{CO})_{12}$ .<sup>40,41</sup> Unlike most models of  $[\text{NiFe}]$ -hydrogenases, the trimetallic Schröder complex catalyzes proton reduction. A related trimetallic compound, Compound 3A shown in Scheme 1, is expected to form from the reaction of NiSODA and  $\text{Fe}_3(\text{CO})_{12}$ . The expected metallopeptide features two terminal nitrogen-based ligands to the Ni and two thiolates bridging between the nickel and a diiron-hexacarbonyl fragment. As a test of the ability to utilize the cysteine thiolates of NiSODA as bridging ligands in a heterometallic complex, we synthesized the NiSODA- $\text{Fe}_2(\text{CO})_6$  complex analogue of the Schröder complex

by the reaction at high temperature of NiSODA and  $\text{Fe}_3(\text{CO})_{12}$  in a mixture of methanol and water. After reaction, the NiSODA- $\text{Fe}_2(\text{CO})_6$  complex was purified by analytical HPLC (Supporting Information, Figure S3), and all spectroscopic measurements were performed with purified samples. ESI-MS was used to confirm that the mass of the isolated product matched that of the anticipated trimetallic complex (Supporting Information, Figure S4). In addition to the anticipated molecular ion (1010.6  $m/z$  for  $[\text{M-H}]^-$ ), several heavier peaks were also observed in the mass spectrum. These peaks are likely the result of air oxidation of the thiols. This process may be accelerated by the harsh ionization conditions employed for ESI-MS. However, we also note that not all species are detected with equal efficiency via ESI-MS so that peak intensities cannot be correlated with relative concentrations in the sample. Peaks associated with the loss of several CO ligands, commonly observed for metal carbonyls, were also detected. Furthermore, the modeled isotope pattern for each set of peaks, uniquely determined by the isotopic abundances of each of the elements in the complex, closely matches the experimental data. Thus there can be little doubt that the complex contains all three metals. The Ni/Fe ratio of the purified metalloprotein was determined to be 1:2.1 via metal quantitation using ICP-MS. This result again confirms the expected metal composition.

Figure 2 compares the UV–vis spectra of Ni-SODA and NiSODA- $\text{Fe}_2(\text{CO})_6$ . A strong metal-to-ligand charge transfer (MLCT) band around 335 nm and a weak d-d transition at 470 nm (Supporting Information, Figure S6) are seen in the spectrum of NiSODA- $\text{Fe}_2(\text{CO})_6$  but not in the Ni-SODA starting material.<sup>42</sup> This pair of features is commonly associated with the so-called butterfly Fe–S core of an  $(\mu\text{-SR})_2\text{Fe}_2(\text{CO})_6$  fragment. Since we have previously shown that  $\text{Fe}_3(\text{CO})_{12}$  can react with two cysteines in peptides to form  $\text{Fe}_2(\text{RS})_2(\text{CO})_6$ , we considered it necessary to ensure that the diiron butterfly core complex did not arise simply from SODA- $\text{Fe}_2(\text{CO})_6$ , that is, a nickel-free complex.<sup>30</sup> As a control,  $\text{Fe}_3(\text{CO})_{12}$  was reacted with SODA, that is, without a coordinated Ni, to establish whether an SODA- $\text{Fe}_2(\text{CO})_6$  complex could be formed. The dotted line in Figure 2 demonstrates that indeed, a diiron product with the expected UV–vis features was formed. As shown in Supporting Information, Figure S5, the retention time of this nickel-free, diiron complex (42 min) is substantially different from the trimetallic peptide (30 min). Additionally, the charge transfer band was shifted to slightly lower energy (328 to 334 nm) for SODA- $\text{Fe}_2(\text{CO})_6$  relative to the trimetallic NiSODA- $\text{Fe}_2(\text{CO})_6$  complex. Thus considering together the UV–vis, mass spectroscopic, and metal quantitation data, we conclude that the reaction with NiSODA did result in trimetallic peptide. We attribute the subtle shift in the about 330 nm charge transfer band of the trimetallic to the altered electronic environment created by sharing the electron density of the sulfurs with the neighboring Ni ion. Furthermore, based on the presence of this charge transfer band, there can be no doubt that the  $\text{Fe}_2(\text{CO})_6$  fragment is coordinated to the cysteinyl sulfurs.

Figure 3 compares the CD spectra of Ni-SODA, NiSODA- $\text{Fe}_2(\text{CO})_6$ , and SODA- $\text{Fe}_2(\text{CO})_6$  in the visible region. The CD spectrum of NiSODA consists of a negatively signed feature at 475 nm and two positive features at higher energies. The negatively signed feature is unchanged in the spectrum of NiSODA- $\text{Fe}_2(\text{CO})_6$ , but the positive features are shifted to higher energy and an additional one has emerged. It is worth

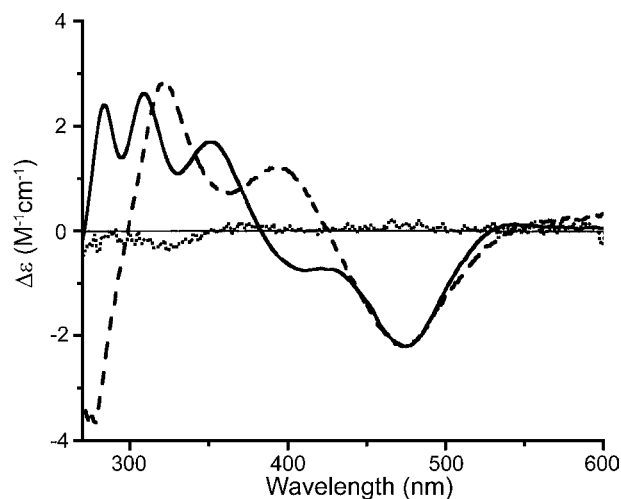


**Figure 3.** CD spectra from NiSODA (dashed line), [NiSODA- $\text{Fe}_2(\text{CO})_6$ ] (solid line), and SODA- $\text{Fe}_2(\text{CO})_6$  (dots) in NEM buffer (50 mM, pH 7.5). The buffer solution alone is shown in gray.

noting that the spectrum of SODA- $\text{Fe}_2(\text{CO})_6$  is completely flat, providing additional evidence for a trimetallic product in the reaction of NiSODA with  $\text{Fe}_3(\text{CO})_{12}$ . Neupane and co-workers reported the spectra for NiSODA and related nickel-containing peptides with several variations at the N-terminus,<sup>38</sup> and the spectrum of NiSODA matches that reported. It is consistent with a chiral, square planar  $\text{N}_2\text{S}_2$  environment for the nickel (Figure 3). Neupane and co-workers demonstrated that the negatively signed feature is an excellent reporter on the nature of the nitrogen coordination; it shifts dramatically ( $2,150\text{ cm}^{-1}$ ) upon conversion of the terminal amine to an amide producing a bis-amide coordination sphere.<sup>43</sup> The observation that this feature is virtually unchanged by addition of the  $\text{Fe}_2(\text{CO})_6$  fragment to NiSODA suggests that the nitrogen coordination of the nickel is relatively unchanged in the trimetallic complex. On the other hand, the positive features have been attributed to sulfur-based transitions. The dramatic change in this region of the CD spectrum provides additional evidence that coordination of the  $\text{Fe}_2(\text{CO})_6$  fragment occurs through the cysteinyl sulfurs.

FTIR spectroscopy has proven invaluable for characterizing metal carbonyls in peptides/proteins because there are no interfering peptide vibrations at similar frequencies (ca.  $2000\text{ cm}^{-1}$ ). FTIR spectra of [SODA- $\text{Fe}_2(\text{CO})_6$ ] and [NiSODA- $\text{Fe}_2(\text{CO})_6$ ] revealed bands at  $2074\text{ cm}^{-1}$ ,  $2038\text{ cm}^{-1}$ , and  $2002\text{ cm}^{-1}$  (Figure 4). These frequencies are nearly identical to those reported for related peptidyl bis-thiolate ligated  $\text{Fe}_2(\text{CO})_6$  complexes,<sup>30,31</sup> and demonstrate conclusively not only that the carbonyl ligands are retained in the products, but also that their bonding to iron is not significantly influenced by the nickel. Additionally, the number and intensities of these bands demonstrate the formation of a complex with pseudo  $C_{2v}$  symmetry.<sup>42</sup> In considering how or if the peptide modifies the properties of the coordinated metalcenter, it is interesting to compare the FTIR spectra of NiSODA- $\text{Fe}_2(\text{CO})_6$  and the analogous tetrathiolate  $\text{Ni}(\text{SR})_2(\mu\text{-SR}')_2\text{Fe}_2(\text{CO})_6$  complex reported by Schröder. The tetrathiolate complex also has an FTIR spectrum with three peaks in the CO vibration region at  $2035$ ,  $1995$ , and  $1955\text{ cm}^{-1}$ . Thus, as expected, both complexes are pseudo  $C_{2v}$  when considering only the  $\text{Fe}_2(\text{CO})_6$  fragment. However, the frequencies of the tetrathiolate complex are systematically shifted by approximately  $40\text{ cm}^{-1}$  to lower

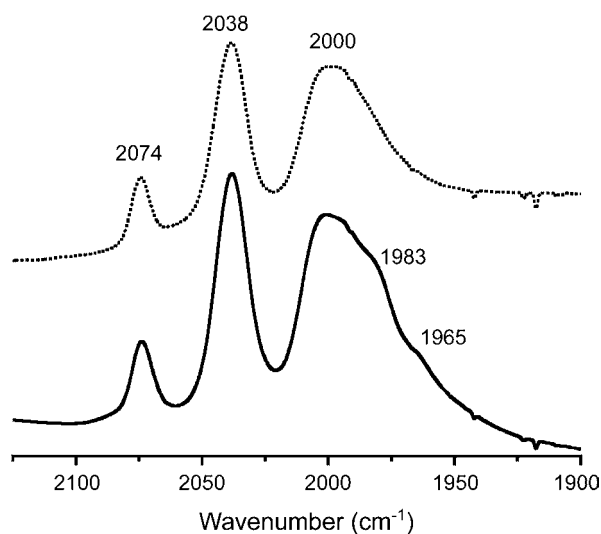


**Figure 4.** FTIR spectra from  $[\text{SODA-Fe}_2(\text{CO})_6]$  (dotted line) and  $[\text{NiSODA-Fe}_2(\text{CO})_6]$  (solid line). The samples were prepared as dried films on a  $\text{CaF}_2$  window.

energy. This can be explained by the significant sharing of electron density between the Ni and Fe parts of the complex. However, those of  $\text{NiSODA-Fe}_2(\text{CO})_6$  are nearly identical to the well-known  $\mu\text{-(S(CH}_2\text{)}_3\text{S)-Fe}_2(\text{CO})_6$  complex and suggest that there is very little electronic interaction between the Ni and the diiron fragments. The question of why there is not appreciable electronic interaction between the Ni and diiron parts of the complex in the peptide then comes naturally to the fore. Although one might ordinarily be tempted to look to the first coordination spheres of the metal, the exchange of the two terminal thiolates at the nickel for amine/amide coordination alone is probably not sufficient for this electronic change. Instead, we hypothesize, that the steric hindrance imposed by the peptide occludes one side of the nickel. The likely effect is that the nickel, bridging sulfur, and iron atoms are no longer coplanar. Instead, the square planar nickel is in one plane, and the bridging thiolates and irons form a second plane. If this assumption is correct, the electronic communication between the nickel and the irons is almost completely severed since each metal interacts with a different orbital of the sulfur.

**NiW and NiMo Complexes.** Darensbourg and co-workers have systematically characterized the electronic and steric parameters of square planar  $\text{NiN}_2\text{S}_2$  complexes as bidentate, S-donor ligands to  $\text{W}(\text{CO})_4$  complexes by comparison of the  $\nu(\text{CO})$  stretching frequencies.<sup>44</sup> By analogy, we have also considered the reaction of NiSODA with  $[\text{M}(\text{CO})_4(\text{piperidine})_2]$  ( $\text{M} = \text{Mo}, \text{W}$ ) to generate heterobimetallic Ni–W and Ni–Mo complexes (Compound 3b in Scheme 1). Analytical HPLC of the reaction mixtures suggested that a single, much slower-running (i.e., more hydrophobic), major product was formed in each reaction (data not shown), and the product could be purified using HPLC (Supporting Information, Figure S7). Although by analogy to previous work we anticipated formation of a bimetallic species by cysteine thiolate substitution of both piperidine ligands, mass spectrometry indicated formation of heavier complexes. As shown in Figure 5 and Supporting Information, Figure S8, modeling of the isotopic distribution patterns observed in the MALDI-TOF spectra suggests that the products contained a single Ni and two Mo or W ions consistent with formation of  $(\mu\text{-NiSODA-}$

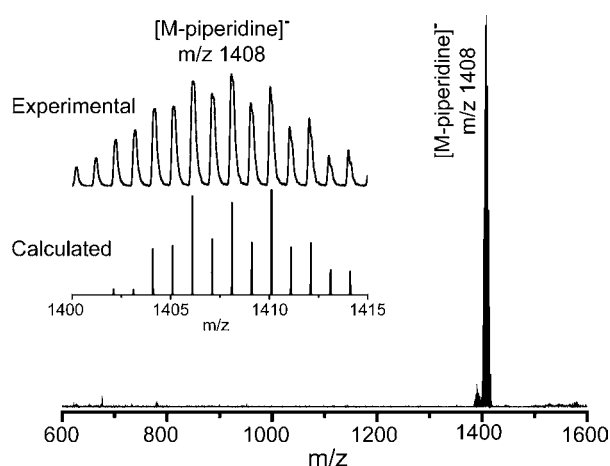


**Figure 5.** Experimental and calculated MALDI-TOF mass spectra for  $\text{NiSODA-}[\text{W}(\text{CO})_4(\text{piperidine})_2]$  in aqueous, 50 mM NEM buffer (pH 7.5) solution (data recorded in negative ion mode). Simulation assumes loss of a single piperidine ligand during ionization.

$\kappa\text{S}:\kappa\text{S}'$ ) $[\text{M}(\text{CO})_4(\text{piperidine})_2]$  complexes. We note that intact parent ions were not detected for the complexes in the mass spectra; instead, ions corresponding to loss of a single piperidine (for W) or four CO ligands (for Mo) from the trimetallic complexes were observed. This is not unusual as the harsh ionization conditions of MALDI often dissociate loosely bound ligands, like carbonyls, from metal complexes. In short, the mass spectra suggest that only a single piperidine ligand was substituted in each reaction to generate a trinuclear cluster. Furthermore, the Ni/M ratios for  $\text{M} = \text{Mo}$  and W were determined to be 1:2.2 and 1:2.0, respectively, using ICP-MS, providing additional evidence for trinuclear complexes.

As was the case for the NiFe complex already described, CD spectra in the visible region demonstrated that the Ni– $\text{N}_2\text{S}_2$  center remained intact in both the Mo and W products, and the sulfur-based transitions were dramatically changed by coordination of a heterometallic fragment (Supporting Information, Figure S9). UV–vis spectroscopy was also used to characterize the electronic environment of both the Ni and the W or Mo heterometal. As shown in Figure 6 and Supporting Information,

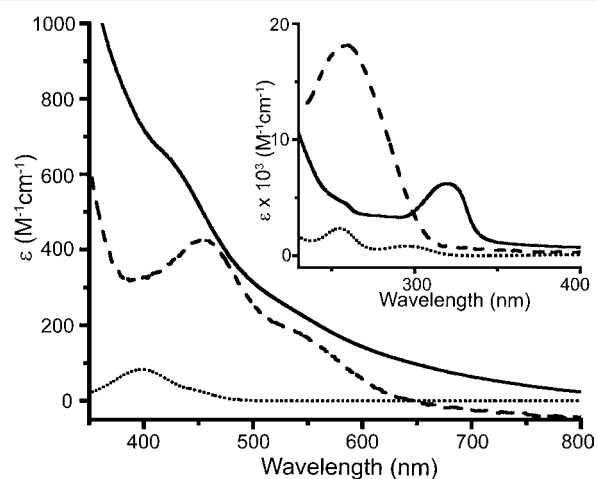


**Figure 6.** UV–vis spectra for NiSODA in 50 mM aqueous NEM buffer solution (dashed line),  $\text{W}(\text{CO})_4(\text{piperidine})_2$  in methanol (dotted line) and  $\text{NiSODA-}[\text{W}(\text{CO})_4(\text{piperidine})_2]$  in 50 mM aqueous NEM buffer solution (solid line).

Figure S10, broad transitions were observed in the spectra of both NiSODA and NiSODA-[M(CO)<sub>4</sub>(piperidine)]<sub>2</sub> (M = W or Mo) at 465 and 550 nm. These features have been described as characteristic of square planar nickel in an N<sub>2</sub>S<sub>2</sub> geometry. Inspection of the remaining features in the UV-vis spectra provides insights into the nature of the bonding of the peptide to the W or Mo fragment. Considering first the spectrum of the W precursor, W(CO)<sub>4</sub>(piperidine)<sub>2</sub>, it consists of two groups of features: a d-d transition visible band at 400 nm and two UV transitions at 255 and 300 nm arising from MLCT bands from the metal d orbitals to the CO π\* orbitals. Since there are two inequivalent sets of CO ligands, trans and cis to the nitrogens, two MLCT transitions are observed. Relative to the strongly σ-donating piperidine ligand, a cysteinyl alkyl thiolate is expected to be weakly σ- and π- donating. Thus replacement of a piperidine by cysteine upon formation of the peptide coordinated complex is expected to raise the energy of the d<sub>π</sub> orbitals and stabilize the d<sub>σ\*</sub> orbitals resulting in red shifts of both the d-d and the MLCT transitions (See also Supporting Information, Figure S11 for a qualitative molecular orbital (MO) diagram of relevant orbitals). As shown in Figure 6, these shifts are observed for NiSODA-[W(CO)<sub>4</sub>(piperidine)]<sub>2</sub> providing strong evidence that the peptide coordinates the W via a thiolate. Additionally, replacement of only one of the piperidine ligands with cysteine, as suggested by the MALDI data, should create three sets of CO ligands since the ligands trans to the peptide and the piperidine are no longer equivalent. The observation of three MLCT bands (at 260, 280, and 320 nm) for NiSODA-[W(CO)<sub>4</sub>(piperidine)]<sub>2</sub> relative to the two seen for the starting material also suggests that only one of the piperidine ligands was exchanged during the reaction. Similar features in the optical spectrum of NiSODA-[Mo(CO)<sub>4</sub>(piperidine)]<sub>2</sub> (Supporting Information, Figure S10) provide evidence that an analogous Mo complex was formed.

Further information regarding the binding mode of the cysteines was obtained by probing the binding energies of the sulfur 2p core electrons in NiSODA and NiSODA-[Mo(CO)<sub>4</sub>(piperidine)]<sub>2</sub> via XPS. Signals corresponding to both oxidized and reduced forms of sulfur could be detected in the samples because of air oxidation, and, for both of these sulfur signals, a 1.0–1.3 eV increase in binding energy was observed upon comparison of NiSODA to the heterometallic complex (Supporting Information, Figure S12, Table S1). This is consistent with the results of Walton and co-workers that the binding energy of an S 2p<sub>3/2</sub> electron increases by at least +0.5 eV upon conversion from a terminal to a bridging position and provides additional evidence that the cysteinyl sulfurs are bridging ligands in NiSODA-[Mo(CO)<sub>4</sub>(piperidine)]<sub>2</sub>.<sup>45,46</sup>

Figure 7A shows an FTIR spectrum from [NiSODA-W(CO)<sub>4</sub>(piperidine)]<sub>2</sub> in the CO stretching region. Several attempts were made to obtain spectra for the Mo complex, but signals were very weak and are thus not discussed here. For [NiSODA-W(CO)<sub>4</sub>(piperidine)]<sub>2</sub>, four strong bands are observed: 2003, 1930, 1885, and 1847 cm<sup>-1</sup>. A weaker band at 1970 cm<sup>-1</sup> was also found. The bands are higher in energy than those of the precursor Mo/W complexes indicating a decrease in metal backbonding into the π\* orbital upon coordination of a poorer electron donor, cysteine thiolate. The presence of these bands confirms retention of the CO ligands in the NiW peptide. Furthermore, according to the arguments below, the number of bands provides additional evidence for formation of a trinuclear complex. In work analogous to that presented here, Ainscough and co-workers described the FTIR

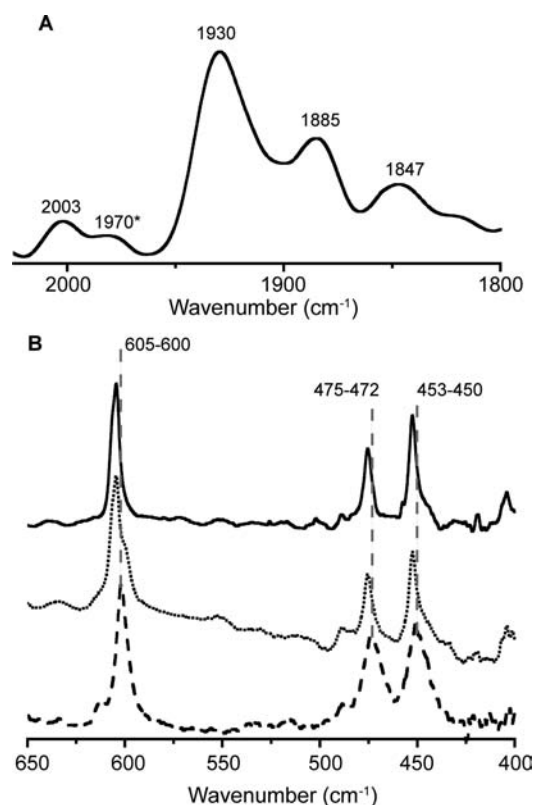


**Figure 7.** FTIR spectra from NiSODA-[W(CO)<sub>4</sub>(piperidine)]<sub>2</sub> (solid line), NiSODA-[Mo(CO)<sub>4</sub>(piperidine)]<sub>2</sub> (dotted line), and NiSODA (dashed line) complexes in the (A) 2025–1800 cm<sup>-1</sup> region and (B) 650–400 cm<sup>-1</sup> region. The spectrum in Panel A was obtained from a dried peptide film on a single CaF<sub>2</sub> window. Because of IR absorption by CaF<sub>2</sub> at low wavenumbers, spectra in Panel B were obtained from samples in KBr pellets.

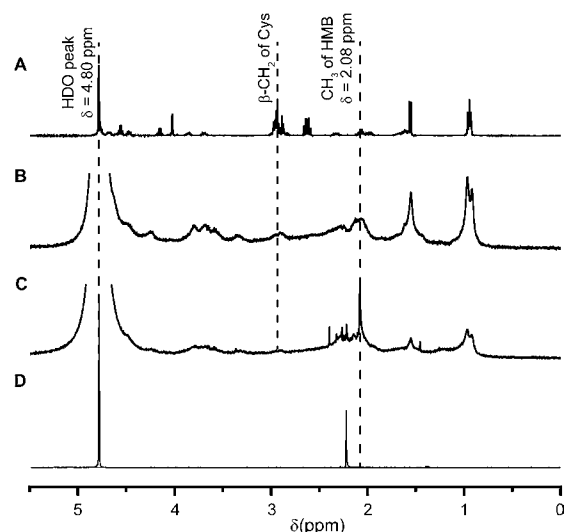
spectra of *cis*-W(CO)<sub>4</sub>XY complexes in which X was an amine and Y a thiolate.<sup>47</sup> These complexes also produced four CO stretching bands at frequencies of approximately 2018, 1900, 1880, and 1845 cm<sup>-1</sup>. Assuming pseudo-C<sub>2v</sub> symmetry about the W, these bands can be assigned as having a<sub>1</sub>, a<sub>1</sub>, b<sub>1</sub>, and b<sub>2</sub> symmetry. Asali and co-workers also described a series of [W(CO)<sub>4</sub>(piperidine)]<sub>2</sub>Z complexes in which Z is a bidentate phosphine or dithiolate ligand.<sup>48–50</sup> These compounds also had four CO stretching frequencies, and it is likely that these are analogous to the strong bands observed in our experiment. We assign the weaker 1970 cm<sup>-1</sup> band found in our spectrum to the single asymmetric stretch anticipated for a *trans*-W(CO)<sub>4</sub>XY complex.<sup>51,52</sup>

Figure 7B shows the FTIR spectra from [NiSODA-M(CO)<sub>4</sub>(piperidine)]<sub>2</sub> (M = Mo, W) and NiSODA in the region 400–650 cm<sup>-1</sup>. NiSODA has three vibrations in this region at 600, 472, and 450 cm<sup>-1</sup>. Two of these (472 and 450 cm<sup>-1</sup>) are believed to arise from Ni–N stretching and the third (600 cm<sup>-1</sup>) from out-of-plane bending of the C=O of the coordinated amide.<sup>53,54</sup> These bands were systematically shifted to higher wavenumbers to 605, 475, and 453 cm<sup>-1</sup> upon coordination of the Mo or W fragment. This suggests that sharing of electron density through the bridging sulfurs impacts the strengths of the Ni–N bonds. In short, the Mo/W fragment is expected to withdraw electron density from the Ni–S bonds. The Ni fragment then compensates with stronger Ni–N bonding as reflected in the IR stretches.

Although not the intended reaction products, the trimetallic clusters generated here are not without precedent in the literature. A similar trimetallic ( $\mu\text{-N}_2\text{S}_2\text{-}\kappa\text{S}'$ )[W(CO)<sub>5</sub>]<sub>2</sub> has been reported.<sup>55</sup> In the case of reactions with NiSODA, it is likely there are both steric and thermodynamic reasons for the formation of trimetallic Ni-M (M = Mo, W) complexes as opposed to binuclear ones. First, the transition state for a 1:1 reaction between NiSODA and [M(CO)<sub>4</sub>(piperidine)<sub>2</sub>] (M = Mo, W) may require accommodating both the bulky side chains of the SODA peptide and the not-yet-displaced piperidine ligands in a structure that is too sterically cramped to be energetically accessible. On the thermodynamic side, it is important to consider that piperidine is a strong  $\sigma$ -donating ligand, but the alkyl thiolate sulfurs are expected to be relatively weak  $\sigma$ - and  $\pi$ -donating ligands. Thus, replacement of both piperidine ligands may be enthalpically unfavorable. Similarly, tethering of both sides of the Mo or W complex to the peptide in a 1:1 complex should cause a substantial decrease in entropy that will also favor the 1:2 reaction. On the other hand, it is natural to also ask why, in contrast, our Ni–Ru reactions (described below) produced bimetallic complexes. In these reactions, water ligands on the Ru precursor complex are replaced by the relatively stronger  $\sigma$ -donating cysteine thiolates providing a much greater enthalpic driving force. Substitution of the water molecules by cysteinates from the ruthenium fragment also increases the entropy of the system.

**NiRu Complexes.** Two related, dinuclear Ni–Ru(arene) complexes were identified as synthetic targets: [NiSODA-Ru( $\eta^6$ -*p*-cymene)(H<sub>2</sub>O)](NO<sub>3</sub>)<sub>2</sub> and [NiSODA-Ru( $\eta^6$ -C<sub>6</sub>Me<sub>6</sub>)(H<sub>2</sub>O)](NO<sub>3</sub>)<sub>2</sub> (Compound 3C in Scheme 1). As described by Ogo and co-workers, analogous complexes utilizing the *N,N'*-dimethyl-*N,N'*-bis(2-mercaptoethyl)-1,3-propanediamine ligand as an N<sub>2</sub>S<sub>2</sub> coordination environment for the nickel were highly water-soluble and, in the case of the hexamethylbenzene complex, cleaved hydrogen to form a bridging hydride species.<sup>6</sup>

NiRu complexes were generated by the reaction of NiSODA in NEM buffered aqueous solution (pH 7.5) with [Ru( $\eta^6$ -arene)(H<sub>2</sub>O)<sub>3</sub>](NO<sub>3</sub>)<sub>2</sub> where the arene was either hexamethylbenzene or *p*-cymene. The hexamethylbenzene complex was then purified for further analysis via reverse-phase analytical HPLC (Chromatogram is shown in Supporting Information, Figure S13). MALDI-TOF spectra of the reaction products showed that complexes of the expected molecular weights were formed (*m/z* = 996 and 969 for hexamethylbenzene and *p*-cymene complexes, respectively). Furthermore, these spectra had the isotope pattern expected for a heterobimetallic Ni–Ru complex (Supporting Information, Figure S14), and the Ni/Ru ratio determined via ICP-MS was 1:0.9. Figure 8 shows <sup>1</sup>H NMR spectra for SODA, NiSODA, [NiSODA-Ru( $\eta^6$ -C<sub>6</sub>Me<sub>6</sub>)(H<sub>2</sub>O)](NO<sub>3</sub>)<sub>2</sub>, and the ruthenium precursor used in synthesis of the heterometallic complex. As shown in Figure 8B, binding of Ni to SODA resulted in a broadening and shifting in particular of the resonances of the  $\beta$ -protons of the cysteines confirming interaction of the cysteinyl sulfurs with Ni. Upon addition of the Ru-hexamethylbenzene fragment, a sharp resonance at 2.08 ppm appeared that can be attributed to the resonance of the methyl-protons of the hexamethylbenzene ring (Figure 8C), providing further evidence that this ligand was retained in the product. The position of this methyl resonance was shifted from 2.22 ppm in the starting compound to 2.08 ppm in the product. Interestingly, Ogo and colleagues also reported that the methyl resonance shifted upfield in their



**Figure 8.** <sup>1</sup>H NMR spectra of (A) SODA, (B) NiSODA, (C) [NiSODA-Ru( $\eta^6$ -C<sub>6</sub>Me<sub>6</sub>)(H<sub>2</sub>O)](NO<sub>3</sub>)<sub>2</sub>, and (D) [Ru( $\eta^6$ -C<sub>6</sub>Me<sub>6</sub>)(H<sub>2</sub>O)<sub>3</sub>](SO<sub>4</sub>) in D<sub>2</sub>O. Chemical shifts were referenced to the solvent (HDO) peak at  $\delta$  = 4.80 ppm.

analogous NiRu complex to 2.15 or 2.18 ppm depending on the counterion present.<sup>6</sup> Thus, it is likely that the Ru fragments in that organometallic complex and in the peptide reported here are in similar electronic environments.

UV–vis, CD, and FTIR spectroscopy were also used to characterize the electronic environment of the products. Figure 9 shows the UV–vis spectrum of the heterobimetallic (NiRu)

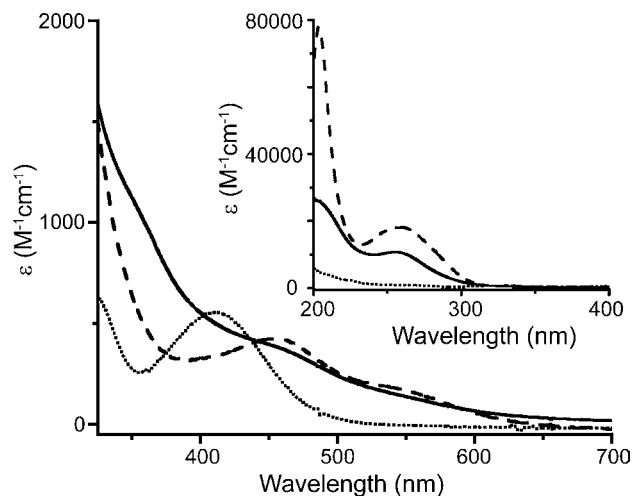


**Figure 9.** UV–visible spectra for NiSODA (dashed line), [Ru( $\eta^6$ -C<sub>6</sub>Me<sub>6</sub>)(H<sub>2</sub>O)<sub>3</sub>](NO<sub>3</sub>)<sub>2</sub> (dotted line), and [NiSODA-Ru( $\eta^6$ -C<sub>6</sub>Me<sub>6</sub>)(H<sub>2</sub>O)](NO<sub>3</sub>)<sub>2</sub> (solid line). Spectra were obtained at pH 7.5 in 50 mM NEM buffer. The inset shows the absorbance in the UV region.

hexamethylbenzene complex, and data from the *p*-cymene complex can be found in the Supporting Information, Figure S15. Although the spectra of the heterobimetallic complexes consist of a superposition of relatively broad peaks especially in the visible region, features arising primarily from each of the individual metal fragments were observed and help to confirm retention of the expected ligand sets. For example, the broad transitions observed at 460 and 545 nm are characteristic of Ni in a square planar N<sub>2</sub>S<sub>2</sub> geometry and are also seen in the

spectrum of the starting NiSODA complex. Similarly, the band centered at 400 nm is likely to arise from a Ru-based ligand field (LF) transition.<sup>56</sup> Despite shared features between the precursor complexes and the heterobimetallic complexes, it is important to note that the spectrum from the bimetallic complex is not simply a linear combination of the spectra of the individual components. Instead, the precise maximum of each feature is shifted by interaction of the two metal fragments. For example, the 400 nm band in the heterobimetallic complex is blue-shifted relative to the starting Ru-arene complex likely because of interaction of the Ru fragment with the sulfur ligands. The CD spectra for the heterobimetallic NiRu complexes are shown in Supporting Information, Figure S16. As for the other compounds described in this work, the negative feature at 475 nm was unchanged by binding of the Ru-fragments, shifting only 5 nm to lower energy. However, the higher energy positive features were significantly changed providing evidence that the Ru fragment is coordinated via the sulfur ligands. Finally, as described for the Mo/W complexes, the Ni–N stretching modes of the NiRu complexes were slightly higher in energy than those of NiSODA (Supporting Information, Figure S17).

## CONCLUDING REMARKS

We have demonstrated that NiSODA reacts with a range of heterometallic fragments with different metals, nuclearities, and ligand sets to form peptide-coordinated hydrogenase mimics. Spectroscopic evidence suggests that in all cases the N<sub>2</sub>S<sub>2</sub> coordination of the Ni is maintained and the sulfurs are the reactive sites, forming bridges to the heterometallic fragment. Additionally, the unique vibrational frequencies of metal carbonyls can be used to demonstrate incorporation of heterometallic fragments and evaluate the donor ability of the nickel fragment. This synthetic approach is similar to that reported for other [NiFe]-hydrogenase small molecule mimics, and opens countless opportunities to construct water-soluble hydrogenase mimics and compare their properties to those of both the enzymes and the small molecules. Furthermore, this method parallels the biosynthesis of the hydrogenase active site, believed to proceed via incorporation of the Fe fragment with its diatomic ligands into the apoenzyme followed by transfer of the Ni atom from a metallochaperone to complete the active site.<sup>57</sup> This suggests that a model peptide could be used as an *in vitro* substrate for biosynthetic studies.

Hydrogenases are not the only known heterometallic enzymes. In fact, this group includes a number of bioenergetically and technologically important enzymes catalyzing small molecule transformations such as acetylcoenzyme A synthase-carbon monoxide dehydrogenase (ACS-CODH),<sup>58–60</sup> nitrogenase,<sup>61,62</sup> and the oxygen evolving complex (OEC) of photosystem II.<sup>63,64</sup> There is significant interest in developing bioinspired, homogeneous, molecular catalysts corresponding to each of these enzymes, and this work provides a starting point for constructing peptide-based mimics. Peptide-based systems offer several crucial advantages over traditional models including the opportunity to alter the aqueous solubility of relevant inorganic complexes<sup>30,31,65</sup> and the chance to tailor functionally important outer coordination sphere interactions.<sup>34</sup> In particular, there are remarkable parallels between our synthetic hybrid bioinorganic/organometallic site and the acetylcoenzyme A synthase (ACS) active site, the A-cluster. That center consists of a [4Fe4S] cluster bridged to a binuclear center. The nickel site distal to the iron–sulfur cluster has very

similar coordination to the nickel to NiSODA, consisting of two cysteinyl and two amide nitrogen ligands. Interestingly, the metal binding site proximal to the iron–sulfur cluster can be variously occupied by a nickel, copper, or zinc ion sharing the cysteinyl sulfurs with the distal nickel in the same arrangement as the complexes that were constructed in this work.<sup>59,66</sup> In essence, the distal site can be thought of as a metallosynthon for coordination of heterometallic fragments. By analogy, our results may have direct relevance also to the biosynthesis of ACS-CODH, and it may be the case that the proximal metal site in ACS-CODH can be used to coordinate novel metalcenters creating new bioinorganic/organometallic catalysts with unique reactivities.

In this work, we have created five distinct heterometallic peptides. In the cases of the NiRu and NiFe peptides, complexes analogous to the known small molecules were formed. However, in the cases of the reactions with Mo and W fragments, unexpected trinuclear complexes were formed because of both steric and thermodynamic constraints imposed by the peptide. This suggests that reactions of even small metallopeptides may have novel products, and metallopeptides will serve as crucial models for metalloprotein catalysis.

## ASSOCIATED CONTENT

### Supporting Information

Additional mass spectral, UV–vis, CD, and XPS data. HPLC chromatograms. Partial molecular orbital diagram. This material is available free of charge via the Internet at <http://pubs.acs.org>.

## AUTHOR INFORMATION

### Corresponding Author

\*E-mail: [jonesak@asu.edu](mailto:jonesak@asu.edu). Phone: 480-965-0356. Fax: 480-965-2747.

### Notes

The authors declare no competing financial interest.

## ACKNOWLEDGMENTS

This research was supported through the Center for Bio-Inspired Solar Fuel Production, an Energy Frontier Research Center funded by the U.S. Department of Energy, Office of Science, Office of Basic Energy Sciences under Award Number DE-SC0001016. A.D. also thanks the Science Foundation of Arizona for a graduate fellowship. We thank Dr. Gwenyth Gordon in the W. M. Keck Foundation Laboratory for Environmental Biogeochemistry for completing ICP-MS analyses, as well as the LeRoy Eyring Center for Solid State Science and Dr. Tim Katcher for performing the XPS experiments.

## REFERENCES

- (1) Cammack, R.; Frey, M.; Robson, R. *Hydrogen as a fuel, learning from Nature*; Taylor and Francis: London, U.K., 2001.
- (2) Fontecilla-Camps, J. C.; Volbeda, A.; Frey, M. *Trends Biotechnol.* **1996**, *14*, 417–420.
- (3) Volbeda, A.; Charon, M. H.; Piras, C.; Hatchikian, E. C.; Frey, M.; Fontecilla-Camps, J. C. *Nature* **1995**, *373*, 580–587.
- (4) Ohki, Y.; Tatsumi, K. *Eur. J. Inorg. Chem.* **2011**, 973–985.
- (5) Canaguier, S.; Artero, V.; Fontecave, M. *Dalton Trans.* **2010**, 315–325.
- (6) Ogo, S.; Kabe, R.; Uehara, K.; Kure, B.; Nishimura, T.; Menon, S. C.; Harada, R.; Fukuzumi, S.; Higuchi, Y.; Ohhara, T.; Tamada, T.; Kuroki, R. *Science* **2007**, *316*, 585–587.

- (7) Chalbot, M.-C.; Mills, A. M.; Spek, A. L.; Long, G. J.; Bouwman, E. *Eur. J. Inorg. Chem.* **2003**, 453–457.
- (8) Hsieh, C.-H.; Chupik, R. B.; Brothers, S. M.; Hall, M. B.; Darensbourg, M. Y. *Dalton Trans.* **2011**, 40, 6047–6053.
- (9) Zhu, W.; Marr, A. C.; Wang, Q.; Neese, F.; Spencer, D. J. E.; Blake, A. J.; Cooke, P. A.; Wilson, C.; Schröder, M. *Proc. Natl. Acad. Sci. U.S.A.* **2005**, 102, 18280–18285.
- (10) Li, Z.; Ohki, Y.; Tatsumi, K. *J. Am. Chem. Soc.* **2005**, 127, 8950–8951.
- (11) Carroll, M. E.; Barton, B. E.; Gray, D. L.; Mack, A. E.; Rauchfuss, T. B. *Inorg. Chem.* **2011**, 50, 9554–9563.
- (12) Liebgott, P.-P.; de Lacey, A. L.; Burlat, B.; Cournac, L.; Richaud, P.; Brugna, M.; Fernandez, V. M.; Guigliarelli, B.; Rousset, M.; Léger, C.; Dementin, S. *J. Am. Chem. Soc.* **2011**, 133, 986–997.
- (13) McIntosh, C. L.; Germer, F.; Schulz, R.; Appel, J.; Jones, A. K. *J. Am. Chem. Soc.* **2011**, 133, 11308–11319.
- (14) Goris, T.; Wait, A. F.; Saggu, M.; Fritsch, J.; Heidary, N.; Stein, M.; Zebger, I.; Lenzian, F.; Armstrong, F. A.; Friedrich, B.; Lenz, O. *Nat. Chem. Biol.* **2011**, 7, 310–318.
- (15) Iranzo, O.; Chakraborty, S.; Hemmingsen, L.; Pecoraro, V. L. *J. Am. Chem. Soc.* **2011**, 133, 239–251.
- (16) Korendovych, I. V.; Senes, A.; Kim, Y. H.; Lear, J. D.; Fry, H. C.; Therien, M. J.; Blasie, J. K.; Walker, F. A.; DeGrado, W. F. *J. Am. Chem. Soc.* **2010**, 132, 15516–15518.
- (17) Shiga, D.; Nakane, D.; Inomata, T.; Funahashi, Y.; Masuda, H.; Kikuchi, A.; Oda, M.; Noda, M.; Uchiyama, S.; Fukui, K.; Kanaori, K.; Tajima, K.; Takano, Y.; Nakamura, H.; Tanaka, T. *J. Am. Chem. Soc.* **2010**, 132, 18191–18198.
- (18) Lu, Y.; Yeung, N.; Sieracki, N.; Marshall, N. M. *Nature* **2009**, 460, 855–862.
- (19) Nanda, V.; Koder, R. L. *Nat. Chem.* **2010**, 2, 15–24.
- (20) Koder, R. L.; Anderson, J. L. R.; Solomon, L. A.; Reddy, K. S.; Moser, C. C.; Dutton, P. L. *Nature* **2009**, 458, 305–309.
- (21) Reddi, A. R.; Guzman, T. R.; Breece, R. M.; Tiemey, D. L.; Gibney, B. R. *J. Am. Chem. Soc.* **2007**, 129, 12815–12827.
- (22) Kennedy, M. L.; Gibney, B. R. *J. Am. Chem. Soc.* **2002**, 124, 6826–6827.
- (23) Xie, F.; Sutherland, D. E. K.; Stillman, M. J.; Ogawa, M. Y. *J. Inorg. Biochem.* **2010**, 104, 261–267.
- (24) Zastrow, M. L.; Peacock, A. F. A.; Stuckey, J. A.; Pecoraro, V. L. *Nat. Chem.* **2012**, 4, 118–123.
- (25) Laplaza, C. E.; Holm, R. H. *J. Am. Chem. Soc.* **2001**, 123, 10255–10264.
- (26) Musgrave, K. B.; Laplaza, C. E.; Holm, R. H.; Hedman, B.; Hodgson, K. O. *J. Am. Chem. Soc.* **2002**, 124, 3083–3092.
- (27) de Hatten, X.; Bothe, E.; Merz, K.; Huc, I.; Metzler-Nolte, N. *Eur. J. Inorg. Chem.* **2008**, 4530–4537.
- (28) Fedorova, A.; Chaudhari, A.; Ogawa, M. Y. *J. Am. Chem. Soc.* **2003**, 125, 357–362.
- (29) Green, K. N.; Jeffery, S. P.; Reibenspies, J. H.; Darensbourg, M. Y. *J. Am. Chem. Soc.* **2006**, 128, 6493–6498.
- (30) Jones, A. K.; Lichtenstein, B. R.; Dutta, A.; Gordon, G.; Dutton, P. L. *J. Am. Chem. Soc.* **2007**, 129, 14844–14845.
- (31) Roy, S.; Shinde, S.; Hamilton, G. A.; Hartnett, H. E.; Jones, A. K. *Eur. J. Inorg. Chem.* **2011**, 1050–1055.
- (32) Apfel, U.-P.; Kowol, C. R.; Morera, E.; Görls, H.; Lucente, G.; Keppler, B. K.; Weigand, W. *Eur. J. Inorg. Chem.* **2010**, 5079–5086.
- (33) Sano, Y.; Onoda, A.; Hayashi, T. *Chem. Commun.* **2011**, 47, 8229–8231.
- (34) Jain, A.; Lense, S.; Linehan, J. C.; Rauegi, S.; Cho, H.; DuBois, D. L.; Shaw, W. *J. Inorg. Chem.* **2011**, 50, 4073–4085.
- (35) Choudhury, S. B.; Lee, J.-W.; Davidson, G.; Yim, Y.-I.; Bose, K.; Sharma, M. L.; Kang, S.-O.; Cabelli, D. E.; Maroney, M. J. *Biochemistry* **1999**, 38, 3744–3752.
- (36) Wuerges, J.; Lee, J.-W.; Yim, Y.-I.; Yim, H.-S.; Kang, S.-O.; Carugo, K. D. *Proc. Natl. Acad. Sci. U.S.A.* **2004**, 101, 8569–8574.
- (37) Barondeau, D. P.; Kassmann, C. J.; Bruns, C. K.; Tainer, J. A.; Getzoff, E. D. *Biochemistry* **2004**, 43, 8038–8047.
- (38) Neupane, K. P.; Gearty, K.; Francis, A.; Shearer, J. *J. Am. Chem. Soc.* **2007**, 129, 14605–14618.
- (39) Ellman, G. L. *Arch. Biochem. Biophys.* **1958**, 74, 443–450.
- (40) Wang, Q.; Barclay, J. E.; Blake, A. J.; Davies, E. S.; Evans, D. J.; Marr, A. C.; McInnes, E. J. L.; McMaster, J.; Wilson, C.; Schröder, M. *Chem.—Eur. J.* **2004**, 10, 3384–3396.
- (41) Perra, A.; Davies, E. S.; Hyde, J. R.; Wang, Q.; McMaster, J.; Schröder, M. *Chem. Commun.* **2006**, 1103–1105.
- (42) Works, C. F. *J. Chem. Educ.* **2007**, 84, 836–838.
- (43) Neupane, K. P.; Shearer, J. *Inorg. Chem.* **2006**, 45, 10552–10566.
- (44) Rampersad, M. V.; Jeffery, S. P.; Golden, M. L.; Lee, J.; Reibenspies, J. H.; Darensbourg, D. J.; Darensbourg, M. Y. *J. Am. Chem. Soc.* **2005**, 127, 17323–17334.
- (45) Best, S. A.; Brant, P.; Feltham, R. D.; Rauchfuss, T. B.; Roundhill, D. M.; Walton, R. A. *Inorg. Chem.* **1977**, 16, 1976–1979.
- (46) Srinivasan, V.; Stiefel, E. I.; Elsberry, A.; Walton, R. A. *J. Am. Chem. Soc.* **1979**, 101, 2611–2614.
- (47) Ainscough, E. W.; Brodie, A. M.; Larsen, N. G.; Stevens, M. R. *Inorg. Chim. Acta* **1981**, 50, 215–220.
- (48) Asali, K. J.; El-Khateeb, M.; Musa, M. M. *J. Coord. Chem.* **2002**, 55, 1199–1207.
- (49) El-khateeb, M.; Asali, K. J.; Musa, M. M. *Transition Met. Chem.* **2002**, 27, 163–165.
- (50) Asali, K.; El-khateeb, M.; Salhab, R. *Transition Met. Chem.* **2003**, 28, 544–547.
- (51) Goff, S. E. J.; Nolan, T. F.; George, M. W.; Poliakov, M. *Organometallics* **1998**, 17, 2730–2737.
- (52) Darensbourg, D. J.; Burch, R. R.; Darensbourg, M. Y. *Inorg. Chem.* **1978**, 17, 2677–2680.
- (53) Condrate, R. A.; Nakamoto, K. *J. Chem. Phys.* **1965**, 42, 2590–2598.
- (54) Kincaid, J. R.; Nakamoto, K. *Spectrochim. Acta* **1976**, 32A, 277–283.
- (55) Jeffery, S. P.; Singleton, M. L.; Reibenspies, J. H.; Darensbourg, M. Y. *Inorg. Chem.* **2006**, 46, 179–185.
- (56) Weber, W.; Ford, P. C. *Inorg. Chem.* **1986**, 25, 1088–1092.
- (57) Böck, A.; King, P. W.; Blokesch, M.; Posewitz, M. C. Maturation of hydrogenases. In *Advances in Microbial Physiology*; Poole, R. K., Ed.; Elsevier: New York, 2006; Vol. 51, pp 1–71.
- (58) Doukov, T. I.; Iverson, T. M.; Seravalli, J.; Ragsdale, S. W.; Drennan, C. L. *Science* **2002**, 298, 567–572.
- (59) Darnault, C.; Volbeda, A.; Kim, E. J.; Legrand, P.; Vernede, X.; Lindahl, P. A.; Fontecilla-Camps, J. C. *Nat. Struct. Biol.* **2003**, 10, 271–279.
- (60) Svetlitchnyi, V.; Dobbek, H.; Meyer-Klaucke, W.; Meins, T.; Thiele, B.; Römer, P.; Huber, R.; Meyer, O. *Proc. Natl. Acad. Sci. U.S.A.* **2004**, 101, 446–451.
- (61) Rees, D. C. *Annu. Rev. Biochem.* **2002**, 71, 221–246.
- (62) Howard, J. B.; Rees, D. C. *Proc. Natl. Acad. Sci. U.S.A.* **2006**, 103, 17088–17093.
- (63) Zouni, A.; Witt, H.-T.; Kern, J.; Fromme, P.; Krauss, N.; Saenger, W.; Orth, P. *Nature* **2001**, 409, 739–743.
- (64) Umena, Y.; Kawakami, K.; Shen, J.-R.; Kamiya, N. *Nature* **2011**, 473, 55–60.
- (65) Gale, E. M.; Cowart, D. M.; Scott, R. A.; Harrop, T. C. *Inorg. Chem.* **2011**, 50, 10460–10471.
- (66) Drennan, C. L.; Doukov, T. I.; Ragsdale, S. W. *J. Biol. Inorg. Chem.* **2004**, 9, 511–515.